Journal of Photopolymer Science and Technology
Volume 29, Number 6 (2016) 809 − 816 ©2016SPST

Requirement for Suppression of Line Width Roughness in Fabrication of Line-and-Space Patterns with 7 nm Quarter-Pitch Using Electron Beam Lithography with Chemically Amplified Resist Process

Takahiro Kozawa

The Institute of Scientific and Industrial Research, Osaka University, 8-1 Mihogaoka, Ibaraki, Osaka 567-0047, Japan

The suppression of line width roughness (LWR) is the most difficult task in the development of resist materials used for sub-10 nm fabrication. We have investigated the feasibility of the fabrication of line-and-space patterns with 7 nm quarter-pitch (7 nm space width and 28 nm pitch) with a chemically amplified resist process, assuming electron beam (EB) lithography. In this study, we investigated the requirement for suppressing LWR to 10 and 20% critical dimension (CD), using the simulation on the basis of the reaction mechanisms of chemically amplified EB resists. The simulation results suggested that the suppression of LWR to 20% CD is feasible, while 10% CD LWR is away from the current status of chemically amplified resists.
Keywords: EB lithography, chemically amplified resist, line width roughness, sensitivity, sub-8 nm

1. Introduction

The reduction in the critical dimension (CD) of semiconductor devices has been pursued to meet the market demand for low-cost devices. The reduction will continue and is expected to reach sub-8 nm half-pitch in 2025. According to the International Technology Roadmap for Semiconductors (ITRS) published by the Semiconductor Industry Association, extreme ultraviolet (EUV) lithography with double patterning (DP), EUV extensions such as a high-NA, directed self-assembly (DSA) extension, nanoimprint lithography (NIL), and maskless lithography (ML2) are potential solutions for sub-8 nm half-pitch fabrication of micro processing unit (MPU) fin and flash memory. For dynamic random access memory (DRAM) and MPU metal level, EUV extension with DP, EUV with quadruple patterning (QP), DSA extension, NIL, and ML2 are potential solutions. Besides ML2, the requirements for electron beam (EB) lithography have also become stricter with the increasing demand for high-resolution semiconductor lithography tools, because EB lithography is an indispensable technology for the production of photomasks, EUV masks, and NIL molds. In particular, the requirement for the fabrication of NIL molds is severe, because 1× molds are used in NIL unlike 4× reduction photomasks for optical lithography. The fabrication of molds is an important issue for the realization of sub-8 nm fabrication with NIL[1-3].

In previous studies [4-8], the feasibility of sub-8 nm fabrication with a chemically amplified EB resist process was investigated, assuming the line-and-space patterns with 7 nm half-pitch. The relationship between line edge roughness (LER) and sensitivity was theoretically investigated in the beam size (or blur) range of 3-7 nm, assuming the latest EB mask writer (NuFlare Technology EBM-9000

Received October 19, 2016
Accepted November 26, 2016

[9]). LER estimated on the basis of current resist performance was away from the requirement [4,5]. The design of chemically amplified resists capable of resolving 7 nm half-pitch line-and-space patterns is, if not impossible, difficult from the viewpoint of the suppression of LER as long as the current resist materials and EB mask writer are assumed. Then, the feasibility of 7 nm space delineation was investigated by extending the pitch from 14 to 28 nm, considering the application of double patterning technology. Hereafter, such pattern (7 nm space width and 28 nm pitch) is called the line-and-space pattern with 7 nm quarter-pitch. LER was calculated on the basis of the sensitization and reaction mechanisms of chemically amplified EB resists. By extending the pitch to 28 nm while keeping the space width at 7 nm, LER was significantly suppressed. The fabrication of line-and-space patterns with 7 nm quarter-pitch by EB lithography is considered to be promising.

In this study, we investigated the feasibility of the suppression of line width roughness (LWR) to 10 and 20% CD, using the simulation on the basis of the reaction mechanisms of chemically amplified EB resists. The relationship between LWR and LER is expressed as $LER \approx LWR/\sqrt{2}$. LER is inversely proportional to the normalized chemical gradient [the gradient of normalized protected unit concentration after postexposure baking (PEB) in the direction vertical to the line pattern] [10-12]:

$$LER = \frac{f_{LER}}{dm/dx} \quad (1)$$

Here, m, dm/dx, and f_{LER} are the protected unit concentration normalized by its initial value before PEB, the normalized chemical gradient, and a proportionality constant (development factor), respectively. For the key parameters that determine LER, the probable parameter ranges have been reported on the basis of the analysis of the line-and-space patterns fabricated with one-fourth exposure duty of an electron beam [7]. In that study [7], the validity of the simulation has been also examined. This experiment was carried out using one of highest-resolution chemically amplified EB resists, the resolution of which is 15.5 nm half-pitch [13]. The probable parameter ranges were 0.1-0.3 nm for the effective reaction radius for deprotection and 0.4-0.7 for the development factor [7]. Using these parameters, the requirement for suppressing LWR to 10 and 20% CD is discussed.

2. Simulation Model and Method

The beam profile I_b(x: perpendicular to a line pattern) was approximated using the Gaussian function,

$$I_b(x) = I_{b0} \exp\left(-\frac{x^2}{2\sigma_b^2}\right) \quad (2)$$

where I_{b0} and σ_b are the exposure dose and beam size, respectively. The beam size ($1\sigma_b$) was changed from 1.0 to 2.0 nm in steps of 0.2 nm. The acceleration voltage of electron beam was assumed to be 50 kV. The exposed area was pitch × 1000 nm^2. The pitch was set to 28 nm. Electrons were randomly injected into the target area in accordance with the beam profile expressed by Eq. (2). The injected electrons randomly collided with resist molecules in accordance with the stopping power. The trajectories of secondary electrons and the reaction of thermalized electrons with acid generators were calculated in accordance with the reported procedure.[4] Poly(4-hydroxystyrene) (PHS) was assumed as the backbone polymer for chemically amplified resists. The thermalization distance of secondary electrons in PHS has been reported to be 3.2 nm [14]. The acid generator concentration was set to 20 and 30 wt% in triphenylsulfonium-triflate (TPS-Tf) equivalent. The initial protection ratio was assumed to be 30%. The decrease in acid yield caused by the protection of the hydroxyl groups of the resist polymer was taken into account. The deprotonation efficiency of protected unit radical cations was set to a typical value of 0.3 [15].

The preneutralization of acids before PEB [16,17] was assumed because an annealing-type resist is generally used in EB lithography. Using the acid distribution after the preneutralization as the initial condition, the catalytic chain deprotection during PEB was calculated by solving the reaction-diffusion equations for acids and quenchers. In a simple simulation model employing the reaction-diffusion equations, the dynamics of acids and quenchers are

expressed as [18-21]

$$\frac{\partial C_{acid}}{\partial t} = \nabla\left(D_{acid}\nabla C_{acid}\right) - k_n C_{acid} C_q \quad (3)$$

$$\frac{\partial C_q}{\partial t} = \nabla\left(D_q \nabla C_q\right) - k_n C_{acid} C_q \quad (4)$$

where C_{acid}, C_q, D_{acid}, D_q, and k_n represent the concentrations of acids and quenchers, the diffusion constants of acids and quenchers, and the rate constant for neutralization, respectively. D_{acid} was assumed to be 1 nm^2 s^{-1}, for simplicity. Note that the acid diffusion constants of current high-performance resists have been evaluated to be 2−10 nm^2 s^{-1} [22-26]. D_q was assumed to be 0 nm^2 s^{-1}. It has been reported that a low quencher diffusion constant is considered to be preferable from the viewpoint of process control for the line-and-space pattern with 7 nm quarter-pitch [6]. By solving Eqs. (3) and (4), the temporal change in acid concentration was calculated. The temporal change in protected unit concentration was calculated using

$$\frac{\partial C_p}{\partial t} = -k_p C_{acid} C_p \quad (5)$$

Here, C_p and k_p represent the concentration of protected units and the rate constant of deprotection, respectively. The rate constant is expressed as $k_p=4\pi R_p D_{acid}$. Here, R_p is the effective reaction radius for deprotection. The effective reaction radius for deprotection was set to be 0.1-0.3 nm [7]. The parameters used in the simulation are summarized in Table 1 [7,14,15,27,28]. The backscattering coefficient was tentatively assumed to be 0.0 and 0.4. Other details of the reaction mechanisms have been reported elsewhere [29].

Table 1. Parameters used in simulation.

Parameter	Value
Acceleration voltage of electron beam (kV)	50
Beam size (σ_b) (nm)	1.0-2.0
Backscattering coefficient	0, 0.4
Pitch (nm)	28
Resist thickness (nm)	15
Stopping power (eV nm^{-1})	0.769
Resist film density (g cm^{-3}) [27]	1.2
Thermalization distance (nm) [14]	3.2
Acid generator concentration (wt%)	20, 30
Reaction radius of acid generator (nm) [14]	0.70
Effective reaction radius for neutralization (nm)	0.5
Effective reaction radius for deprotection (nm) [7]	0.1-0.3
Protection ratio (%)	30
Deprotonation efficiency of proton source [28]	1.0
Deprotonation efficiency of nonproton source [15]	0.3
Diffusion constant of acids (nm^2 s^{-1})	1.0
Diffusion constant of quenchers (nm^2 s^{-1})	0
PEB time (s)	600

3. Results and Discussion

After the calculation of the sensitization process of acid generators, the subsequent chemical reactions during PEB were calculated to a PEB time of 600 s, which is a typical PEB time for mask fabrication. The normalized chemical gradient of line-and-space patterns with 7 nm quarter-pitch was estimated at x=±3.5 nm for different quencher concentrations. Figure 1 shows the PEB time dependence of the relationship between quencher concentration and normalized chemical gradient. The dashed lines represent the maximum normalized chemical gradient at x=±3.5 nm for each quencher concentration. In the high-quencher-concentration region, the normalized chemical gradient was independent of PEB time (>120 s) for the cases shown in Fig. 1. The results shown in Fig. 1(a) were calculated without the effect of the electrons scattered backward from the substrate. The normalized chemical gradient was maximized at the quencher concentration of 0.13 nm^{-3}. The maximum value was 0.185 nm^{-1}. The results calculated with the backscattering coefficient of 0.4 are shown in Fig. 1(b). The optimum quencher concentration increased to 0.15 nm^{-3} and the maximum value of normalized chemical gradient slightly decreased to 0.182 nm^{-1}. Before the discussion about the effect of backscattered electrons, the dependence of normalized chemical gradient on the acid generator concentration is discussed.

It is known that LER is inversely proportional to the sensitivity [10-12]. By decreasing the sensitivity (increasing the exposure dose), LER is decreased. However, it is also known that there is the lower limit for LER (LER floor) when the sensitivity decreased [30,31]. The main reason for the lower limit of LER is that the concentration of acid generator is finite [32]. Figure 2

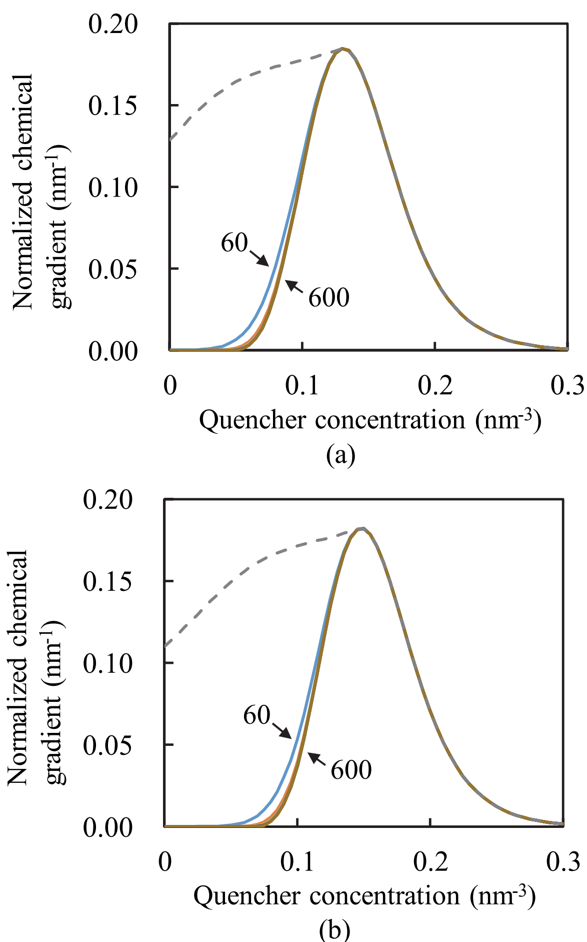

Fig. 1. PEB time dependence of normalized chemical gradient of line-and-space patterns with 7 nm quarter-pitch upon 200 μC cm^{-2} EB exposure. The backscattering coefficients were (a) 0.0 and (b) 0.4. The beam size was 1.6 nm. The acid generator concentration was 30 wt%. The effective reaction radius for deprotection was 0.2 nm. The numerical values in the graph denote PEB time in second, which was changed from 60 to 600 s in steps of 60 s. The dashed lines represent the maximum chemical gradient obtained for each quencher concentration (horizontal axis).

shows the sensitivity dependence of normalized chemical gradient of line-and-space patterns with 7 nm quarter-pitch, which was calculated without the backscattered electrons. The numerical values in the graph denote the acid generator concentration in wt%. Figure 2 indicates that LER reached the floor at the sensitivities of 250, 350, and 450 mJ cm^{-2} for the acid generator concentration of 10, 20, and 30 wt%, respectively. The maximum values of normalized chemical gradient were 0.130, 0.192, and 0.227 nm^{-1} for the acid generator concentration of 10, 20, and 30 wt%, respectively. The maximum normalized chemical gradient can be increased, by increasing the acid generator concentration. However, the increase of acid generator concentration also has negative impacts on the resist performance. For example, the increase of protected unit concentration is required for the suppression of stochastic effects [33,34]. The increase of acid generator concentration leads to the decrease of protected unit concentration due to the exclusion volume effects. Therefore, the acid generator concentration should be adjusted as low as possible, depending on the acceptable sensitivity from the viewpoint of the throughput of mask fabrication. The results shown in Fig. 2 indicates that the realistic optimum acid generator concentrations are roughly 10, 20, and 30 wt% for the acceptable sensitivities of 100, 200, and 300 μC cm^{-2}, respectively, for the beam size of 1.6 nm.

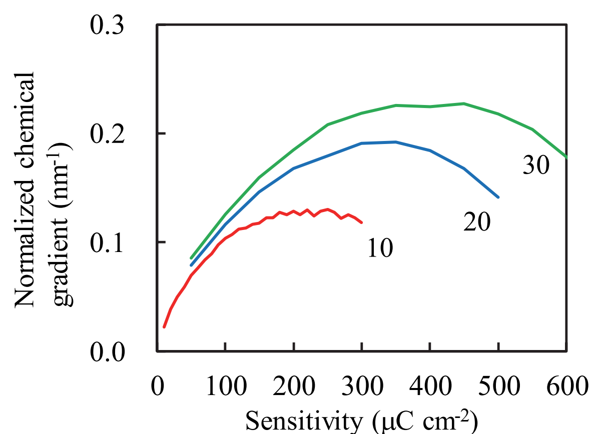

Fig. 2. Sensitivity dependence of normalized chemical gradient of line-and-space patterns with 7 nm quarter-pitch. The backscattering coefficient was 0.0. The beam size was 1.6 nm. The numerical values in the graph denote the acid generator concentration in wt%. The effective reaction radius for deprotection was 0.2 nm. The quencher concentration was optimized to maximize the chemical gradient for each parameter set. The graph for 10 wt% acid generator concentration has been reported in Ref. 8.

Figure 3 shows the effect of backscattered electrons. The sensitivity dependence of normalized chemical gradient of line-and-space patterns with 7 nm quarter-pitch was calculated with and without

the effect of backscattered electrons. The effect of backscattered electrons reaches roughly several tens of μm around the target pattern [35-37]. In other words, the additional energy is uniformly added to the accumulated energy distribution of the target pattern when its size is on the nanometer scale. With such additional energy, acids are uniformly generated around the target pattern. It has been reported that the neutralization between acids and quenchers occurs before PEB even at room temperature in the annealing-type chemically amplified resists [38,39]. Such preneutralization cancels the effect of backscattered electrons. Therefore, the maximum normalized chemical gradients for the cases with and without the effect of backscattered electrons did not significantly differ when the quencher concentration was optimized, as shown in Fig. 1. However, the backscattered electrons decompose the acid generator molecules and decrease the effective concentration for the patterning. Figure 3 indicates the decrease of maximum normalized chemical gradient caused by the decrease in the effective concentration of acid generators. The maximum values of normalized chemical gradient without the effect of backscattered electrons were 0.179, 0.227, and 0.254 nm^{-1} for the effective reaction radius for deprotection of 0.1, 0.2, and 0.3 nm, respectively. In the presence of backscattered electrons, the maximum values of normalized chemical gradient decreased to 0.166, 0.213, and 0.239 nm^{-1} for the effective reaction radius for deprotection of 0.1, 0.2, and 0.3 nm, respectively. The difference between the cases with and without the effect of backscattered electrons was also marked in the low sensitivity region (>400 μC cm^{-2}).

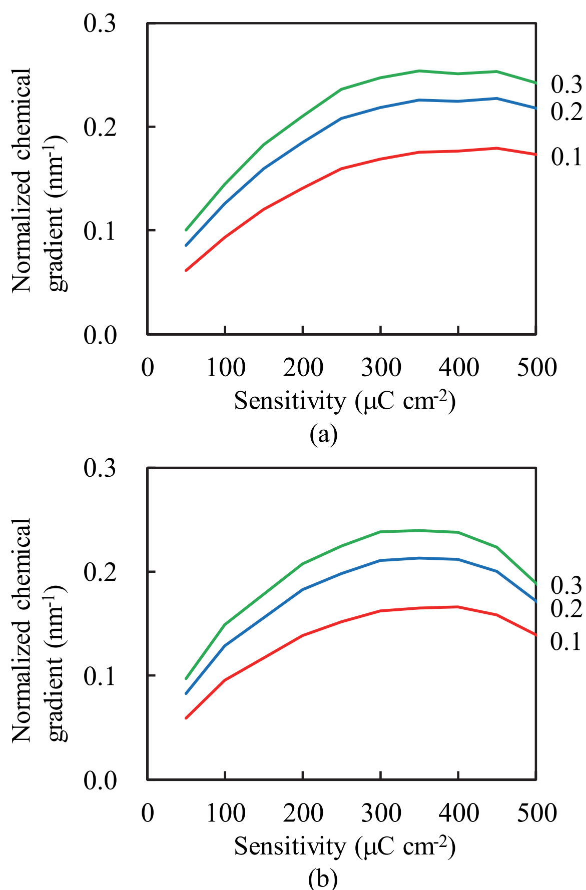

Fig. 3. Sensitivity dependence of normalized chemical gradient of line-and-space patterns with 7 nm quarter-pitch. The numerical values in the graph denote the effective reaction radius for deprotection in nm. The backscattering coefficients were (a) 0.0 and (b) 0.4. The beam size was 1.6 nm. The acid generator concentration was 30 wt%. The quencher concentration was optimized to maximize the chemical gradient for each parameter set.

Figure 4 shows the sensitivity dependence of normalized chemical gradient of line-and-space patterns with 7 nm quarter-pitch, calculated by changing the beam size from 1.0 to 2.0 nm in steps of 0.2 nm. The dashed lines labeled "20% CD LWR" represent the normalized chemical gradient required to suppress LWR to 20% CD. Those upper and lower lines were calculated with the development factors of 0.7 and 0.4 [7], respectively. The effective reaction radius for deprotection has been estimated to be in the range of 0.1-0.3 nm, using one of highest-resolution chemically amplified EB resists [7]. Figures 4(a) and 4(b) show the cases for the effective reaction radii of 0.1 and 0.3 nm, respectively. Figure 4, therefore, indicates that 20% CD LWR cannot be achieved when the performance of current highest-resolution chemically amplified EB resists is assumed. The development factors of EUV resists have been similarly investigated, using the highest performance EUV resists. They range from 0.14 to 0.31 [22-26]. The dashed lines labeled "Ref" in Fig. 4 represent the normalized chemical gradient required for 20% CD LWR, calculated with the development factors of 0.14 and 0.31. The simulation results suggest that LWR of line-and-space patterns with 7

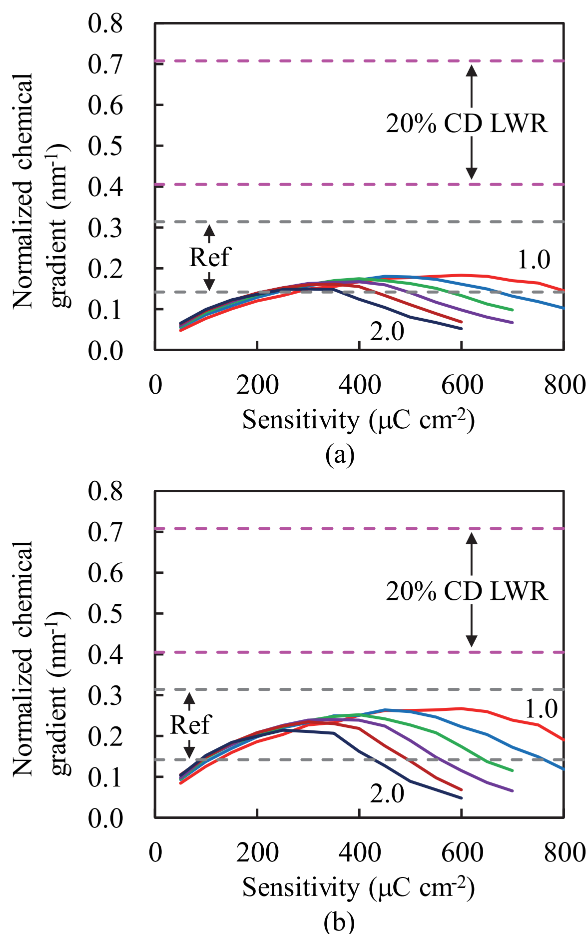

Fig. 4. Sensitivity dependence of normalized chemical gradient of line-and-space patterns with 7 nm quarter-pitch. The numerical values in the graph denote the beam size, which was changed from 1.0 to 2.0 nm in steps of 0.2 nm. The effective reaction radii for deprotection were (a) 0.1 and (b) 0.3 nm. The backscattering coefficients was 0.4. The acid generator concentration was 30 wt%. The quencher concentration was optimized to maximize the chemical gradient for each parameter set. The dashed lines labeled "20% CD LWR" represent the normalized chemical gradient required to suppress LWR to 20% CD. See text for the dashed lines labeled "Ref".

nm quarter-pitch is reduced to 20% CD, if the development factor of chemically amplified EB resists can be decreased to that of chemically amplified EUV resists. The achievable sensitivity depended on the beam size, the effective reaction radius for deprotection, and the development factor, as shown in Fig. 4. The sensitivity of 100 μC cm^{-2} was in the feasible range. The normalized chemical gradient required to suppress LWR to 10% CD is 0.81-1.41 and 0.28-0.63 for the development factors of 0.4-0.7 and 0.14-0.31, respectively. Therefore, 10% CD LWR is away from the current status of chemically amplified resists.

Figure 5 shows the beam size dependence of normalized chemical gradient of line-and-space patterns with 7 nm quarter-pitch, calculated with the acid generator concentration of 30 wt%. The relationship between beam size and normalized chemical gradient depended on the sensitivity, as reported previously [8]. The optimum beam size also depended on the acid generator concentration. In the case of the acid generator concentration of 10 wt% [8], the optimum beam size in terms of LER was around 1.6 nm for the sensitivity of 100-200 μC cm^{-2}. At the sensitivity of 300 μC cm^{-2}, the optimum beam size decreased to 1.2 nm. In the case of the acid generator concentration of 30 wt%, as shown in Fig. 5, the optimum beam sizes were >2.0, 1.6, 1.4, and <1.0 nm for the sensitivities of 100, 200-300, 400, and 500 μC cm^{-2}, respectively. With the increase of acid generator concentration, the optimum beam size for each sensitivity slightly increased.

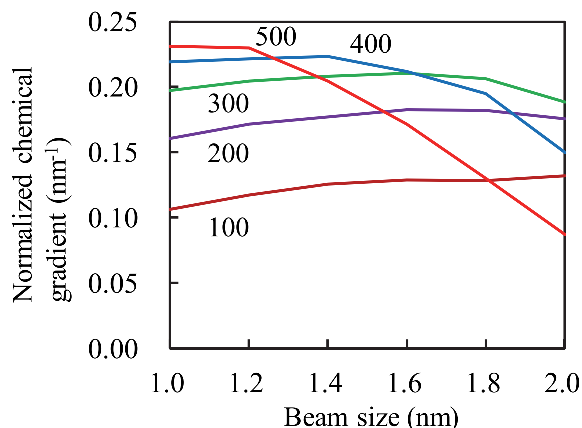

Fig. 5. Beam size dependence of normalized chemical gradient of line-and-space patterns with 7 nm quarter-pitch. The numerical values in the graph denote the sensitivity in μC cm^{-2}, which was changed from 100 to 500 μC cm^{-2} in steps of 100 μC cm^{-2}. The backscattering coefficients was 0.4. The acid generator concentration was 30 wt%. The effective reaction radius for deprotection was 0.2 nm. The quencher concentration was optimized to maximize the chemical gradient for each parameter set.

4. Conclusion

The requirement for suppressing LWR of line-and-space patterns with 7 nm quarter-pitch to 10 and 20% CD was investigated, using the simulation on the basis of chemically amplified EB resists. The suppression of LWR to 10% CD was away from the current status of chemically amplified resists. The suppression of LWR to 20% CD was feasible. For 20% CD LWR, the development factor should be decreased near 0.2. The acid generator concentration is considered to have to be increased near 30 wt% in TPS-Tf equivalent. The achievable sensitivity depended on the beam size and the effective reaction radius for deprotection, and the development factor.

References

1. T. Higashiki, T. Nakasugi, and I. Yoneda, *Proc. SPIE*, **7970** (2011) 797003.
2. W. Zhou, G. Min, J. Zhang, Y. Liu, J. Wang, Y. Zhang, and F. Sun, *Nano-Micro Lett.*, **3** (2011) 135.
3. H. Lan and H. Liu, *J. Nanosci. Nanotechnol.*, **13** (2013) 3145.
4. T. Kozawa, *Jpn. J. Appl. Phys.*, **54** (2015) 056501.
5. T. Kozawa, *Jpn. J. Appl. Phys.*, **54** (2015) 096501.
6. T. Kozawa, *Jpn. J. Appl. Phys.*, **54** (2015) 096703.
7. T. Kozawa, *Jpn. J. Appl. Phys.*, **55** (2016) 056503.
8. T. Kozawa, *Jpn. J. Appl. Phys.*, **55** (2016) 106502.
9. H. Takekoshi, T. Nakayama, K. Saito, H. Ando, H. Inoue, N. Nakayamada, T. Kamikubo, R. Nishimura, Y. Kojima, J. Yashima, A. Anpo, S. Nakazawa, T. Iijima, K. Ohtoshi, H. Anze, V. Katsap, S. Golladay, and R. Kendall, *Proc. SPIE*, **9256** (2014) 925607.
10. G. M. Gallatin, *Proc. SPIE*, **5754** (2005) 38.
11. D. Van Steenwinckel, R. Gronheid, F. Van Roey, P. Willems, and J. H. Lammers, *J. Micro/Nanolithogr. MEMS MOEMS*, **7** (2008) 023002.
12. T. Kozawa, H. Oizumi, T. Itani, and S. Tagawa, *Appl. Phys. Express*, **3** (2010) 036501.
13. K. Yagawa, K. Ugajin, M. Suenaga, Y. Kobayashi, T. Motokawa, K. Hagihara, M. Saito, and M. Itoh, *Proc. SPIE*, **9256** (2014) 925608.
14. T. Kozawa and S. Tagawa, *Jpn. J. Appl. Phys.*, **50** (2011) 030209.
15. H. Yamamoto, T. Kozawa, A. Nakano, K. Okamoto, S. Tagawa, T. Ando, M. Sato, and H. Komano, *Jpn. J. Appl. Phys.*, **44** (2005) 5836.
16. K. Natsuda, T. Kozawa, K. Okamoto, and S. Tagawa, *Jpn. J. Appl. Phys.*, **45** (2006) L1256.
17. K. Natsuda, T. Kozawa, K. Okamoto, and S. Tagawa, *Jpn. J. Appl. Phys.*, **46** (2007) 7285.
18. J. Nakamura, H. Ban, K. Deguchi, and A. Tanaka, *Jpn. J. Appl. Phys.*, **30** (1991) 2619.
19. L. Schlegel, T. Ueno, N. Hayashi, and T. Iwayanagi, *J. Vac. Sci. Technol. B*, **9** (1991) 278.
20. W. D. Hinsberg, F. A. Houle, M. I. Sanchez, and G. M. Wallraff, *IBM J. Res. Dev.*, **45** (2001) 667.
21. H. Fukuda, K. Hattori, and T. Hagiwara, *Proc. SPIE*, **4346** (2001) 319.
22. T. Kozawa, H. Oizumi, T. Itani, and S. Tagawa, *Jpn. J. Appl. Phys.*, **49** (2010) 066504.
23. T. Kozawa, H. Oizumi, T. Itani, and S. Tagawa, *Jpn. J. Appl. Phys.*, **49** (2010) 116505.
24. T. Kozawa, H. Oizumi, T. Itani, and S. Tagawa, *Jpn. J. Appl. Phys.*, **50** (2011) 076503.
25. T. Kozawa, H. Oizumi, T. Itani, and S. Tagawa, *Jpn. J. Appl. Phys.*, **50** (2011) 126501.
26. T. Kozawa, J. J. Santillan, and T. Itani, *Appl. Phys. Express*, **6** (2013) 026502.
27. T. Fukuyama, T. Kozawa, S. Tagawa, R. Takasu, H. Yukawa, M. Sato, J. Onodera, I. Hirosawa, T. Koganesawa, and K. Horie, *Appl. Phys. Express*, **1** (2008) 065004.
28. H. Yamamoto, T. Kozawa, A. Nakano, K. Okamoto, Y. Yamamoto, T. Ando, M. Sato, H. Komano, and S. Tagawa, *Jpn. J. Appl. Phys.*, **43** (2004) L848.
29. T. Kozawa and S. Tagawa, *Jpn. J. Appl. Phys.*, **49** (2010) 030001.
30. P. P. Naulleau, C. N. Anderson, J. Chiu, K. Dean, P. Denham, S. George, K. A. Goldberg, B. Hoef, G. Jones, C. Koh, B.

La Fontaine, A. Ma, W. Montgomery, D. Niakoula, J. Park, T. Wallow, and S. Wurm, *J. Vac. Sci. Technol. B*, **27** (2009) 66.
31. C. N. Anderson and P. P. Naulleau, *J. Vac. Sci. Technol. B*, **27** (2009) 665.
32. T. Kozawa, *Jpn. J. Appl. Phys.*, **51** (2012) 06FC01.
33. T. Kozawa, *Jpn. J. Appl. Phys.*, **51** (2012) 126501.
34. T. Kozawa, J. J. Santillan, and T. Itani, *Jpn. J. Appl. Phys.*, **53** (2014) 084002.
35. S. A. Rishton and D. P. Kern, *J. Vac. Sci. Technol. B*, **5** (1987) 135.
36. J. A. McMillan, S. Johnson, and N. C. MacDonald, *J. Vac. Sci. Technol. B*, **7** (1989) 1540.
37. G. Han, M. Khan, Y. Fang, and F. Cerrina, *J. Vac. Sci. Technol. B*, **20** (2002) 2666.
38. K. Asakawa, T. Ushirogouchi, and M. Nakase, *Proc. SPIE*, **2438** (1995) 563.
39. W. D. Hinsberg, F. A. Houle, M. I. Sanchez, M. E. Morrison, G. M. Wallraff, C. E. Larson, J. A. Hoffnagle, P. J. Brock, and G. Breyta, *Proc. SPIE*, **3999** (2000) 148.